The Canadian Mineralogist
Vol. 43, pp. 1605-1618 (2005)

SULFUR *K*-EDGE XANES SPECTROSCOPY: CHEMICAL STATE AND CONTENT OF SULFUR IN SILICATE GLASSES

MICHAEL E. FLEET[§], XIAOYANG LIU, SARAH L. HARMER[¶] AND PENELOPE L. KING

Department of Earth Sciences, University of Western Ontario, London, Ontario N6A 5B7, Canada

ABSTRACT

The chemical state and local environment of sulfur in basaltic glasses from the eastern Galapagos rift and quenched laboratory experiments have been investigated by synchrotron-radiation S *K*-edge X-ray absorption near-edge structure (XANES) spectroscopy, using an energy-selective fluorescence detector. We have also investigated sulfur in melts in the system $6NaAlSiO_4$–CaS–$CaSO_4$ quenched from 1500°C and various reference compounds, using conventional fluorescence yield and total-electron yield (TEY) recording modes. The S *K*-edge XANES spectrum of CaS dissolved in Na-aluminosilicate glass is dominated by a broad singlet edge-feature near 2475 eV, consistent with isolated SCa_n coordination polyhedra in the melt, whereas that of quenched end-member $CaSO_4$-bearing melt is similar to XANES spectra of crystalline sulfates. The linear correlation between relative XANES area and wt% content of sulfur has been used to estimate the content of sulfur in samples of lazurite (5.6–6.3 wt% by EPMA), scapolite-group minerals (0.4 wt%) and the basaltic glasses (0.04–0.15 wt%). The S *K*-edge XANES spectra of basaltic glasses synthesized under reducing (WM and IQF solid oxygen-buffer) conditions are dominated by a single broad absorption peak at 2470–2482 eV in combination with a weak peak or shoulder at 2470–2471 eV, and are reproduced by mixing XANES spectra of FeS and alkaline-earth monosulfides. The S *K*-edge XANES spectra for glasses from the eastern Galapagos rift are also dominated by S^{2-}, but one TEY spectrum shows possible thiosulfate and another, trace sulfate.

Keywords: basaltic glass, chemical state of sulfur, X-ray absorption near-edge structure (XANES) spectroscopy.

SOMMAIRE

L'état chimique et le milieu structural du soufre dans les verres basaltiques provenant du rift oriental de Galapagos et ceux préparés par trempe au laboratoire ont été étudiés au moyen de l'absorption des rayons X en rayonnement synchrotron, plus spécifiquement la spectroscopie de la structure près du seuil *K* du soufre (spectres XANES), en utilisant un détecteur de fluorescence à dispersion d'énergie. Nous avons aussi étudié l'état du soufre dans la phase fondue du système $6NaAlSiO_4$–CaS–$CaSO_4$ à 1500°C et de divers composés de référence, en utilisant le rendement conventionnel de la fluorescence et aussi le mode de rendement dû à la totalité des électrons (TEY). Le spectre XANES du seuil *K* du soufre dans un verre aluminosilicaté à Na contenant le CaS en solution montre une seule absorption floue près de 2475 eV, ce qui concorde avec la présence de polyèdres de coordinence isolés SCa_n dans le liquide, tandis que pour les échantillons de verre trempés contenant $CaSO_4$, les spectres XANES ressemblent à ceux de sulfates cristallins. La corrélation linéaire entre l'aire relative de l'absorption dans le spectre XANES et la proportion de soufre (en %, par poids) a été utilisée pour estimer la teneur en soufre des échantillons de lazurite (5.6–6.3% selon les données de microsonde électronique), des minéraux du groupe de la scapolite (0.4%), et des verres basaltiques (0.04–0.15%). Les spectres XANES du seuil *K* du soufre des verres basaltiques synthétisés en milieu réducteur (tampons solides d'oxygène WM et IQF) contiennent surtout une seule absorption floue à 2470–2482 eV et aussi un faible pic satellite à 2470–2471 eV, et ils sont reproduits par mélange de spectres de FeS et de monosulfures alcalinoterreux. Le seuil *K* du soufre des verres provenant du rift oriental de Galapagos montre que le soufre est aussi surtout sous forme de S^{2-}, mais un spectre TEY montre la présence possible de thiosulfate, et un autre, de sulfate, en traces.

(Traduit par la Rédaction)

Mots-clés: verre basaltique, état chimique du soufre, absorption des rayons X près du seuil *K* (spectroscopie XANES).

[§] *E-mail address*: mfleet@uwo.ca

[¶] *Present address*: CSIRO Manufacturing and Infrastructure Technology, PO Box 4, Woodville, SA 5011, Australia. *E-mail address*: sarah.harmer@csiro.au

INTRODUCTION

Sulfur is an important minor component in magmatic systems, occurring as species dissolved in the silicate melt and vapor phase and as sulfide or sulfate minerals. Degassing of sulfur at near-surface conditions may: (i) contribute sulfur to the atmosphere, (ii) trigger a volcanic eruption, or (iii) result in the formation of a metalliferous ore deposit (*e.g.*, Luhr 1990, Mathez 1976). To better predict how sulfur species will behave in magmatic systems, it is necessary to understand the controls on sulfur solubility and the chemical state of sulfur in silicate melts. The behavior of sulfur in melts, minerals and fluids is complicated by its wide range in oxidation state and chemical affinity. The speciation of sulfur changes primarily as a function of composition (of melt or mineral or vapor) and fugacity of oxygen and sulfur (*e.g.*, Fincham & Richardson 1954, Haughton *et al*. 1974, Katsura & Nagashima 1974, Wallace & Carmichael 1992, Carroll & Webster 1994, Naldrett 1989). In reduced systems, the dissolution of sulfur is strongly dependent on Fe and less dependent on $f(O_2)$ (*e.g.*, Mavrogenes & O'Neill 1999, O'Neill & Mavrogenes 2002), whereas in oxidized systems, it is strongly dependent on $f(O_2)$ (*e.g.*, Clemente *et al*. 1998). Calcium is of subordinate importance in reduced melts (Haughton *et al*. 1974, O'Neill & Mavrogenes 2002), but becomes a significant control on sulfur solubility in some Fe-free systems (*e.g.*, Beerkens & Kahl 2002, Ducea *et al*. 1999, Fincham & Richardson 1954, Mysen & Popp 1980).

In this paper, we use S *K*-edge X-ray absorption near-edge structure (XANES) spectroscopy to investigate the chemical state and local environment of sulfur in glasses and minerals. We take advantage of the enhanced sensitivity for minor and trace amounts of sulfur afforded by an energy-selective fluorescence detector. We examine submarine basaltic–andesitic glasses from the eastern Galapagos rift that were quenched under hydrostatic pressure, basaltic glasses from quenched laboratory experiments on the partitioning of platinum-group elements (PGE), and synthetic Na–Ca-aluminosilicate glasses spiked with minor to major amounts of sulfur. We also re-investigate the relationship between oxidation state of sulfur and energy position of the S *K*-edge feature, to help resolve ambiguity in assignment of features in the 2471–2477 eV spectral range.

BACKGROUND INFORMATION

Geochemical studies on sulfur generally assume that (SO_4^{2-}) (*i.e.*, S^{6+}) is the oxidized species in magmas and other silicate melts, but in most cases, specific analyses have not been made to test for the presence of other species of sulfur (*e.g.*, Carroll & Rutherford 1988) or no other sulfur species have been observed (Paris *et al*. 2001). In contrast, a more recent study suggests that S^{4+} (as SO_3^{2-} or SO_2) may occur in silicate glass inclusions in olivine and fragments of basaltic glass (Bonnin-Mosbah *et al*. 2002) and, in related studies, Métrich *et al*. (2002, 2003) proposed that S^{4+} is the important intermediate species for the degassing of excess sulfur in oxidized and H_2O-rich basaltic arc volcanos.

Synchrotron radiation XANES spectroscopy is a sensitive probe of the local structure and chemical state of sulfur in minerals and chemical compounds (*e.g.*, Sugiura & Muramatsu 1985, Hitchcock *et al*. 1987, Kitamura *et al*. 1988, Vairavamurthy *et al*. 1993a, b, Li *et al*. 1995, Kasrai *et al*. 1996a, Womes *et al*. 1997, Vairavamurthy 1998, Farrell & Fleet 2000, 2001, Paris *et al*. 2001, Farrell *et al*. 2002, Kravtsova *et al*. 2004). In particular, Li *et al*. (1995) showed that the oxidation state of sulfur correlated with a progressive shift to higher energy of the sulfur *K* and $L_{2,3}$ absorption edges, spanning 10–12 eV from sulfides (2–) to native sulfur (0), sulfite (4+) and sulfate (6+). However, this ruler for chemical state of sulfur was complicated for reduced species by an overall shift of about 4 eV in the *K*- and *L*-edges of metal sulfides, which varied from 2469.5 and 161.6 eV for cubanite to 2473.4 and 163.6 eV for sphalerite, respectively, and correlated linearly with increase in the direct energy-band gap. XANES spectroscopy has also been applied to study sulfur in compositionally complex natural materials, such as coal (Huffman *et al*. 1991, Kasrai *et al*. 1996a), petroleum (Waldo *et al*. 1991) and related hydrocarbons (Sarret *et al*. 1999), humic acids (Beauchemin *et al*. 2002), and glass inclusions trapped in olivine of volcanic rocks (Bonnin-Mosbah *et al*. 2002, Métrich *et al*. 2002, 2003), as well as synthetic silicate glasses (Paris *et al*. 2001). For major to minor amounts of sulfur, the relative strength of absorption peaks is proportional to the amount of the different sulfur species present. This relationship is quantitative for *K*-edge XANES spectra of metal sulfide solid-solutions (Farrell & Fleet 2000, 2001, Farrell *et al*. 2002) and minor amounts of sulfur species in coals (Huffman *et al*. 1991).

EXPERIMENTAL METHODS

Data on glasses investigated in this study are summarized in Tables 1–5. Glass-synthesis experiments in the system $6NaAlSiO_4$–CaS–$CaSO_4$ (LZ40–55; Table 1) were made from starting mixtures of analytical grade CaS (synthetic oldhamite) and anhydrous $CaSO_4$ and a base mixture of ideal nepheline or carnegieite composition ($NaAlSiO_4$; NAS), which was prepared by fritting a stoichiometric mixture of analytical grade Na_2CO_3 and high-purity Al_2O_3 and amorphous SiO_2 in a platinum crucible at 1000°C for about 1 hour. The starting compositions were contained in sealed platinum capsules within sealed evacuated silica-glass tubes; the charges were heated at 1500°C for 15 minutes in a box furnace, and quenched in air and water. The products were characterized by optical microscopy, powder X-ray diffraction and electron-probe micro-analysis

(EPMA). For the EPMA, we used the JEOL JXA–8600 electron microprobe at UWO operated at 15 kV, 10 nA (measured on a Faraday cup), defocused beam, counting times of 15 s for Na and 20 s for other elements, and mineral standards (albite for Na, Al and Si, diopside for Ca and anhydrite for S; Table 2). Sulfur recorded in Table 2 was measured separately, at 15 kV, 11 nA, with a defocused beam and anhydrite as the standard.

The synthetic basaltic glasses were prepared in previous studies (Fleet *et al.* 1999; unpublished work at UWO) by melting an alkali olivine basalt from Iceland (UWO2). Fleet *et al.* (1999) investigated the partitioning of PGE and Au between immiscible (Fe,Ni)-sulfide liquid and basaltic melt. Their starting materials were contained in alumina crucibles within evacuated sealed silica-glass tubes. The charges were heated at 1300°C for 1–2 hours in the presence of a sulfide–oxide liquid, which was used to monitor $f(O_2)$ and $f(S_2)$, and then

TABLE 1. EXPERIMENTS ON GLASS SYNTHESIS IN THE SYSTEM $6NaAlSiO_4$–CaS–$CaSO_4$[1]

Expt.	Starting composition (molar)	Products
LZ40	6NAS[2] + CaS	glass
LZ42	6NAS + $CaSO_4$	glass + sodalite phase (minor)
LZ50	6NAS + $0.9CaSO_4$ + 0.1CaS	glass + sodalite phase (trace)
LZ51	6NAS + CaS (7.80 wt% CaS)	glass
LZ52	6NAS + 0.8CaS (6.34 wt% CaS)	glass
LZ53	6NAS + 0.6CaS (4.84 wt% CaS)	glass + carnegieite (trace)
LZ54	6NAS + 0.4CaS (3.28 wt% CaS)	glass + carnegieite (minor)
LZ55	6NAS + 0.2CaS (1.67 wt% CaS)	carnegieite + oldhamite (CaS)

1. All experiments were made using welded platinum capsules in sealed silica-glass tubes, heated at 1500°C for 15 minutes; in LZ40, the platinum capsule was embedded in a mixture of carbon black and excess CaS.
2. NAS is $NaAlSiO_4$

TABLE 2. COMPOSITIONS OF GLASS SYNTHESIZED IN THE SYSTEM $6NaAlSiO_4$–CaS–$CaSO_4$ (wt%)[1]

	LZ40	LZ42	LZ50	LZ51	LZ52	LZ53	LZ54	LZ55
SiO_2	40.3	38.8	38.6	38.6	40.5	40.8	40.6	40.4
Al_2O_3	33.8	33.0	33.9	33.7	34.5	34.7	35.0	36.2
CaO	6.4	5.9	6.6	6.6	5.4	4.3	3.1	1.1
Na_2O	17.8	15.8	18.2	18.2	18.6	18.8	18.6	21.1
S	2.7	4.5	5.2	2.55	1.95	1.64	1.06	0.75
Subtotal	101.0	98.0	102.5	99.7	101.0	100.2	98.4	99.6
O≡S	1.3	2.3	2.6	1.3	1.0	0.8	0.5	0.4
Total	99.7	95.7	99.9	98.4	100.0	99.4	97.9	99.2
Ca+S[2]	7.8	7.3	7.3	7.8	6.3	4.8	3.3	1.7
Ca+S[3]	7.3	8.7	9.9	7.3	5.8	4.7	3.3	1.6
S1σ	0.3	3.1	0.9	0.28	0.17	0.15	0.23	0.19
XANES area[4]	-	-	-	1.90	1.47	1.27	0.69	0.34

1. Averages of 10 spots, using defocused beam on the electron microprobe; see Table 1 for experimental details. 2. Total Ca + S added. 3. Total Ca + S recovered by EPMA. 4. Relative area within ~2466.3–2497.8 eV interval.

TABLE 3. COMPOSITION OF SYNTHETIC BASALTIC GLASSES (wt%)[1]

	PG 34	PG 35	PG 160R	PG 162R	PG 165	PG 170	PG 174	PG 175	PG 176
SiO_2	48.86	49.05	45.05	46.64	46.46	46.42	46.35	46.86	46.34
Al_2O_3	15.13	14.71	16.77	19.66	18.27	14.26	15.19	14.01	14.26
TiO_2	2.55	2.56	2.33	2.38	2.45	2.30	2.27	2.32	2.30
MgO	7.49	7.58	8.30	8.09	8.13	8.13	7.93	8.12	8.15
FeO*	6.54	6.35	11.57	7.34	9.11	12.20	11.56	11.43	12.08
MnO	0.17	0.17	0.17	0.18	0.17	0.18	0.18	0.18	0.17
CaO	9.80	9.86	8.81	9.65	8.98	8.83	8.78	8.88	8.86
Na_2O	4.62	4.54	4.03	4.23	4.16	4.16	4.29	4.15	4.16
K_2O	2.09	2.09	1.95	2.06	2.02	1.96	1.97	1.95	1.92
P_2O_5	n.d.	n.d.	1.16	1.17	1.17	1.20	1.19	1.16	1.12
S	0.09	0.08	0.04	0.09	0.05	0.10	0.13	0.15	0.12
Sum	97.34	96.99	100.18	101.49	100.97	99.74	99.84	99.21	99.48
O≡S	0.05	0.04	0.02	0.05	0.03	0.05	0.06	0.08	0.06
Total	97.29	96.95	100.16	101.44	100.94	99.69	99.78	99.13	99.42
Log $f(O_2)$	-9.2	-9.2	-11.5	-11.8	-11.5	-12.0	-12.0	-12.0	-12.0
Log $f(S_2)$	-0.9	-0.9	-0.2	-1.3	-0.5	-2.1	-2.3	-2.1	-2.1

1. averages of 12 spots; n.d. (in P_2O_5): not determined; PG160R–PG176 (Fleet *et al.* 1999). Electron-microprobe data.

TABLE 4. COMPOSITION OF BASALT AND GLASS FROM THE GALAPAGOS RIFT

	Whole Rock by EMPA/XRF/ICP-ES					
	D4-J[1]	994-3A[2]	1652-5[1]	1652-1GR[1]	1652-4[1]	1654-3G[1]
SiO_2 wt%	54.10	55.74	56.50	61.0	58.7	56.4
TiO_2	2.84	2.50	1.82	1.31	2.5	2.27
Al_2O_3	11.90	11.77	11.40	11.3	11.3	12.0
FeO	15.70	15.43	15.70	13.6	15.1	14.8
MnO	-	0.28	0.27	0.24	0.3	0.24
MgO	3.02	2.84	1.63	1.27	1.5	2.39
CaO	8.05	7.54	6.63	5.82	6.8	7.13
Na_2O	3.28	3.26	3.21	3.52	3.5	3.12
K_2O	0.28	0.29	0.36	0.43	0.3	0.38
P_2O_5	0.72	0.36	0.73	0.43		0.59
H_2O			1.38	1.47		1.02
S ppm		4200	1380	975		1159
Cl ppm			3665	4419		3097
Total	99.89	100.43	100.14	100.93	100.0	100.77
	Glasses by EMPA[3]					
	D4-JA	994-3	1652-5	1652-1G		84GTVA
SiO_2	53.03	54.68	55.20	59.52		70.90
TiO_2	2.74	2.44	1.84	1.33		0.67
Al_2O_3	11.82	11.51	11.57	11.40		12.35
Cr_2O_3	0.04	0.03	0.00	0.01		0.01
FeO	15.06	14.73	14.60	13.09		3.79
MnO	0.28	0.25	0.22	0.26		0.14
MgO	3.08	2.49	2.48	1.18		0.47
CaO	8.05	7.36	7.41	5.88		1.89
Na_2O	3.26	3.24	3.14	3.55		4.65
K_2O	0.32	0.35	0.34	0.46		2.22
P_2O_5	0.61	0.59	0.64	0.43		0.12
F	0.00	0.00	0.00	0.00		0.00
Cl	0.26	0.26	0.34	0.46		0.48
Total	98.55	97.93	97.78	97.57		97.69

1. Perfit *et al.* (1999), 2. Perfit *et al.* (1983), 3. averages of six spots; P.L. King, analyst.

quenched in cold water. The two glasses from the unpublished experiments (PG34, PG35) were synthesized from UWO2 in a controlled atmosphere [$f(O_2)$, $f(S_2)$] furnace; about 20 g of basalt powder, contained in an alumina crucible, was equilibrated with PGE-bearing iron sulfide liquid at 1200°C for 48 hours, and quenched in the cool zone of the furnace. Concentrations of the major and minor elements were measured by EPMA using the JEOL JXA–8600 electron microprobe at the University of Alabama (Fleet *et al.* 1999; Table 3). For the natural basaltic glasses from the eastern Galapagos rift, major-element compositions were measured by XRF and ICP–MS (Perfit *et al.* 1983, 1999) and EPMA at UWO using 15 kV, 10 nA, and a 20-μm defocused beam (Table 4). For both synthetic and natural basaltic glasses, the amount of sulfur was measured separately by EPMA at UWO, at 15 kV, 31 nA, using a defocused beam and anhydrous $CaSO_4$ as the standard (Table 5). Following documentation by optical microscopy and EPMA electron back-scattering mapping, PG160R, PG162R, PG34, and PG35 were found to contain rare microblebs (<1 μm) of sulfide, and 84GTVA, micro-inclusions of liquidus oxides and pyroxene, whereas 1652–4 and 1652–1 were partially devitrified. Metal monosulfides (MgS, CaS, $Fe_{0.923}S$) were synthesized by dry reaction in evacuated sealed silica-glass tubes (Farrell & Fleet 2000, 2001, Farrell *et al.* 2002). Mineral samples were obtained from the Dana Mineral Collection at UWO; the two samples of lazurite were hand-separated to exclude contamination by pyrite. Native sulfur was of high purity, and miscellaneous sulfur-bearing compounds (*e.g.*, Table 6, Fig. 1) were either high-purity or analytical grade reagents.

Sulfur *K*-edge XANES spectra were collected at the Canadian Synchrotron Radiation Facility (CSRF), Aladdin storage ring (University of Wisconsin at Madison, Wisconsin). The storage ring operates at either 800 MeV or 1 GeV with a ring current of 60–180 mA or 40–80 mA, respectively; the XANES spectra were not markedly affected by differences in operating energy. The spectra were measured on a double crystal monochromator (DCM) beamline in both total electron yield (TEY) and fluorescence yield (FY) modes as a function of incident photon-energy (Bancroft 1992); the beamline actually collects the current yield (CY), but this has traditionally been referred to as "TEY". The DCM is described by Yang *et al.* (1992). It uses an InSb (111) crystal, and has an energy resolution of about 0.6 eV (FWHM) at 1840 eV; the Darwin width of the crystal corresponds to an energy resolution of 0.9 eV for the S *K* edge. The TEY recording mode probes the near surface and is sensitive to near-surface impurities and alteration, whereas the fluorescence-yield mode is more representative of the bulk material. Maximum sampling depths are estimated to be –700 Å for the TEY mode and several thousand ångströms for the FY mode at the *K* edges of Si, S and P (Kasrai *et al.* 1996a, b, Sarret *et al.* 2002). Thus, collection of spectra in both the TEY and fluorescence-yield modes simultaneously for the same sample provides information on near-surface homogeneity and structural continuity. For XANES

TABLE 5. ESTIMATES OF SULFUR CONTENT OF SOME BASALTIC GLASSES AND SILICATE MINERALS (wt%)

	EPMA[1]	XANES area	
		Peak[2]	Maximum ΔE[3]
Synthetic basaltic glasses (ESF measurements)[4]			
PG34	0.093(10)	0.09	0.10
PG35	0.079(11)	0.10	0.10
PG160R	0.038(5)	0.07	0.08
PG162R	0.091(13)	0.11	0.11
PG165	0.053(10)	0.08	0.08
PG170	0.103(12)	0.10	0.10
PG174	0.129(13)	0.11	0.13
PG175	0.152(17)	-	-
PG176	0.121(19)	0.12	0.13
Natural basaltic glasses (ESF measurements)[4]			
D4-J	0.124(9)	0.21	0.20
994-3	0.114(9)	0.12	0.13
1652-1GR	0.074(7)	0.07	0.07
1652-4	0.114(9)	0.10	0.10
1652-4[5]	0.114(9)	0.11	0.10
1652-5	0.101(11)	0.09	0.08
1654-3G	0.105(7)	0.10	0.11
84GTVA	0.000(0)	0.01	0.01
Silicate minerals (FY measurements)[6]			
Scapolite 1810	0.44	-	0.34
Scapolite 202	0.36	-	0.31
Lazurite 2746	6.26	-	8.18
Lazurite 1343	5.56	-	5.59
LZ52	1.95	-	-

1. Averages of 12 spots (glasses), 8–10 spots (minerals). 2. Area beneath edge peak (within ~2466.3 – 2484.3 eV). 3. Maximum collected area (within ~2466.3 – 2497.8 eV). 4. Normalized against PG175. 5. Duplicate XANES sample. 6. Normalized against LZ52.

TABLE 6. RECENT MEASUREMENTS ON THE POSITION OF THE SULFUR *K*-EDGE IN SOME MINERALS AND COMPOUNDS[1]

Mineral or Compound	Energy (eV)	Mineral or Compound	Energy (eV)
chalcopyrite	2469.5	arsenopyrite	2471.2
$Ni_{0.923}S$ (B8)[2]	2469.7	pyrite	2471.5
$Fe_{0.923}S$ (B8)	2470.0	native sulfur	2472.0[3]
pyrrhotite	2470.0	$Na_2S_2O_3$	2471.4 2480.2
sphalerite	2473.3	Na_2SO_3	2477.8
wurtzite	2473.5	Na_2SO_4	2481.9
CaS (B1)[2]	2474.0 2477.4	$CaSO_4$•$2H_2O$	2481.9
MgS (B1)	2475.1	gypsum	2481.9

1. XANES collected by fluorescence yield.
2. B8 has the NiAs-type structure; B1 has the rock salt structure.
3. standard value.

spectroscopy, differences between TEY and fluorescence-yield modes are attributed to bulk sensitivity and scaling only. As noted in Kravtsova *et al*. (2004), our S *K*-edge XANES spectra of reference sulfur compounds compare very favorably with measurements on a more recent generation of Si (111) monochromator beamlines (*e.g*., Bonnin-Mosbah *et al*. 2002). This is because the core-hole lifetime broadening is significantly greater than the resolution of the Si (111) crystal. Also, the edge feature (or white line) of the XANES spectra is often considerably broadened by fine structure reflecting complexity in the final states. Kravtsova *et al*. (2004) emphasized that no new features were evident in S *K*-edge XANES spectra of metal monosulfides recorded using a Si (111) monochromator.

Samples were crushed, lightly ground and uniformly distributed on double-sided conducting carbon tape affixed to a clean stainless steel disk. DCM measurement conditions for the fluorescence-yield mode included a photon-energy range of at least 2460–2500 eV and a step size of 0.25 eV, with count times determined by counting statistics. Minor to trace amounts of S in the synthetic and natural basaltic glasses were measured using an energy-selective fluorescence (ESF) detector, which has about 10× greater sensitivity than the regular multi-channel-plate fluorescence (FY) detector. The nine detection elements of the ESF detector were all set to the S *K* edge, and their output was summed to yield the measured spectrum. Data reduction and analysis used the BAN data-analysis programme (Tyliszcak 1992) and FORTRAN77 codes. The XANES spectra were normalized against incident intensity (I_o), which was measured simultaneously, and were calibrated to the *K*-edge peak of native S at 2472.0 eV (Fuggle & Inglesfield 1992) after removal of a linear pre-edge background. Spectra of reference compounds were scaled relative to the maximum peak-height at the edge. Sulfur *K*-edge XANES spectra for native sulfur were collected at the beginning of each beam-time session for calibration purposes and showed excellent agreement in respect to relative position and intensity of spectral features. Sulfur contents were estimated from the area of the edge peak after removal of background defined by a trigonometric function that closely approximates the conventional arctangent background function (Farrell & Fleet 2001). The high-energy limit of the "edge feature" was taken variously at 2484.3 and 2497.8 eV (Table 5).

In addition, S *L*-edge XANES were collected on all samples using the CSRF Mark IV Grasshopper monochromator beamline, following operating conditions and procedures described in Kravtsova *et al*. (2004). However, the TEY and FY signals for the basaltic glasses, which contained only 0.00–0.15 wt% S, were too weak for meaningful interpretation, and all of these spectra were discarded. Farrell *et al*. (2002) had earlier noted that even for monosulfide solid-solutions, where sulfur is present as a major constituent, S *L*-edge spectra do not allow quantitative analysis similar to that achieved for corresponding S *K*-edge spectra owing to their greater complexity and a lack of reproducibility of the background.

One sample from the Galapagos rift (D4–J) was investigated by micro-FTIR analysis at UWO, using a Nicolet Magna 850 FTIR spectrometer with a KBr beam splitter, MCT–A detector and a Spectral Tech Continuum microscope. Spectra were obtained with 4 cm^{-1} resolution and 200 scans, and the dry-air-purged background was analyzed prior to the sample. The sample was doubly polished to a 1 μm finish, and cleaned in acetone and isopropyl alcohol. No residues from the mounting and cleaning medium were observed, and the analyzed area was free of bubbles and surface imperfections.

RESULTS AND DISCUSSION

Chemical shift of S K edge and oxidation state of sulfur

The S *K*-edge XANES spectra (Fig. 1) and edge positions (Table 6) of our reference on compounds are similar to those of literature studies (*e.g*., Li *et al*. 1995, Farrell & Fleet 2001, Paris *et al*. 2001, Farrell *et al*. 2002, Bonnin-Mosbah *et al*. 2002). The spectra are characterized by prominent absorption-edge features **a** and **b**, attributed to transition of the S 1*s* core electron to the lowest unoccupied antibonding states on the S atom, and various post-edge features **b**, **c**, **d**, *etc*., generally attributed to multiple scattering resonances, the broad feature **b** having contributions from both sources. Because both initial and final electron-states are important in defining the transition energy associated with the edge feature, the XANES spectrum yields information on the lower part of the conduction band, as well as on the chemical state and local stereochemical environment of the absorber atom. The lowest unoccupied antibonding states on the S atom are restricted by the atom-selection rules $\Delta L = \pm 1$, $\Delta J = 0$ or ± 1. Thus, for most of the present reference compounds [*e.g*., MgS (synthetic niningerite), native sulfur, $Na_2S_2O_3$, Na_2SO_3, and gypsum], the bottom of the conduction band is populated by S 3*s* σ* and S 3*p* σ* orbitals, and the edge feature represents the transition S 1*s* → S 3*p* σ*. Complications arise for sulfides with low-lying empty 3*d* orbitals [transition-metal sulfides and CaS (synthetic oldhamite); Farrell & Fleet 2001, Farrell *et al*. 2002, Kravtsova *et al*. 2004, Soldatov *et al*. 2004]. Although the transition of a 1*s* core electron to unoccupied 3*d* nonbonding and antibonding states is forbidden by the atom-selection rules in the electric dipole approximation ($L = \pm 1$), these forbidden transitions become weakly to strongly allowed at both the metal and S *K* edges of metal sulfides through hybridization of S antibonding and metal 3*d* states (Tossell 1977). This *p–d* hybridization is particularly strong for $3d(e_g)$ states.

As a result, the absorption edge of most transition-metal monosulfides is complex. An initial sharp feature (*e.g.*, **a** in the S *K*-edge XANES of $Fe_{0.923}S$; Fig. 1) represents the transition of S 1*s* electrons to unoccupied S 3*p* σ^* antibonding states hybridized with metal $3d(e_g)$ states (Farrell & Fleet 2001, Soldatov *et al.* 2004); it is also variously referred to elsewhere as the "pre-edge", in analogy with the pre-edge feature of transition-metal *K*-edge XANES, "absorption edge" or "white line". The correspondence of increase in the area of peak **a** with increase in metallic character for NiAs-type Fe–Co–Ni monosulfides, reflecting increase in the number and availability of empty e_g orbitals and covalence of metal–S bonds, is graphic experimental evidence for hybridization of S antibonding and metal 3*d* orbitals (Farrell & Fleet 2001). Indeed, more complex hybridization behavior was recently predicted by calculations of the partial density of states at the bottom of the conduction bands of CoS and NiS (Soldatov *et al.* 2004).

As noted by Li *et al.* (1995), the energy position of the edge feature of S *K*-edge XANES increases progressively and systematically with increase in oxidation state (or mean oxidation state) of the sulfur atom, from 2469.5–2470 eV for transition-metal monosulfides (2–) to 2471 eV for disulfides of the pyrite group (1–), 2472 eV for native sulfur (0), 2478 eV for sulfites, and 2482 eV for sulfates (Fig. 2). Using this chemical shift calibration, Li *et al.* (1995) suggested that the effective oxidation states of the thio and "sulfate" sulfur atoms of sodium thiosulfate appeared to be 1– and 5+, respectively, rather than the commonly assumed values of 2– and 6+. The chemical shift ruler for oxidation state of sulfur works quite well for oxy compounds, where the nearest neighbors of the absorber atom are O^{2-} atoms, and medium- and large-sized cations are restricted to the second or more distant coordination spheres. However, in metal monosulfides, where the sulfur atom is bonded directly to the metal cation, the nature of the metal and the resulting bonding character of the sulfide exert a considerable influence on the position of the S *K* edge. The variation in *K*-edge position from 2469.5 eV for chalcopyrite to 2477 eV for the second edge peak of CaS (Fig. 3), all representing the nominal 2– oxidation state, encompasses the full range of reduced and intermediate oxidation-state for the sulfur species of Figure 2, from S^{2-} to S^{4+}. This broad shift in the S *K*

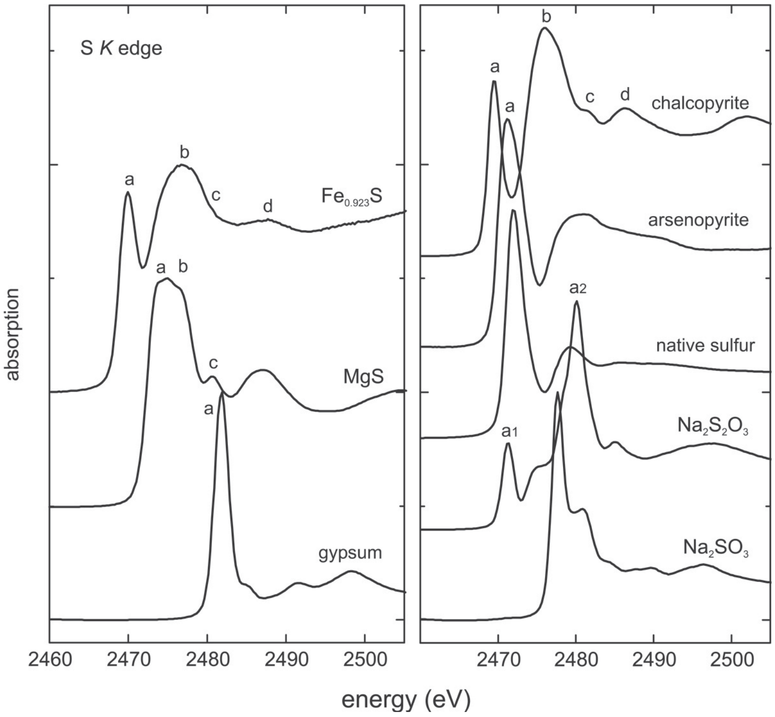

FIG. 1. Sulfur *K*-edge XANES spectra of some reference compounds and minerals, showing, in both left and right panels, a progressive shift of absorption edge to higher energy with increase in oxidation state of sulfur: for sodium thiosulfate, **a1** and **a2** are edge features of reduced and oxidized sulfur atoms, respectively. The spectra were collected in the TEY mode.

edge with change in metal–S bonding character results in considerable ambiguity in the use of S XANES for the recognition of sulfur species in silicate glasses. For this type of application, the overall XANES profile of reference compounds becomes more useful than the actual edge-position for assignment of sulfur speciation. To our knowledge, it is still not possible to extract details of local coordination from XANES spectra of uncharacterized materials, but there have been encouraging advances in the simulation of S *K*- and $L_{2,3}$-edge XANES of alkaline earth and transition-metal monosulfides using multiple scattering theory (Farrell *et al.* 2002, Kravtsova *et al.* 2004, Soldatov *et al.* 2004). A further complication in the interpretation of XANES spectra for glasses using reference compounds is the broadening of features due to the statistical nature of the amorphous structure and the second-order energy shifts of features due to modification of the nearest-neighbor coordination of the absorber atom (*e.g.*, Fleet *et al.* 1997, Fleet & Muthupari 1999).

Quenched 6NaAlSiO$_4$–CaS–CaSO$_4$ melts

The experiments on synthesis of glasses in the system 6NaAlSiO$_4$–CaS–CaSO$_4$ at 1500°C were only partially successful owing to difficulties in retaining volatile sulfur species in the absence of a confining pressure and in either quenching or completely melting some bulk compositions. However, we did obtain end-member-composition glasses for the most commonly encountered sulfur species in magmas, S^{2-}, and near end-member-composition glass for sulfate (S^{6+}; Tables 1, 2, Fig. 4). Glass LZ40 was synthesized from a starting composition of molar (6NAS + 1CaS). Its S *K*-edge XANES spectrum is dominated by a broad singlet edge-feature near 2475 eV, which more or less corresponds to the first-edge peak in the spectrum of crystalline CaS (Fig. 3). The absence of a second peak near 2477 eV in the absorption edge of LZ40 suggests that the second peak in the S *K*-edge XANES of CaS is a multiple scattering feature associated with the extended halite structure. This suggestion was confirmed by Kravtsova *et al.* (2004), who showed that fairly large clusters (consisting of 9 to 13 neighbor shells) of the halite structured CaS are required to simulate the S *K*-edge XANES of CaS using multiple scattering theory. In contrast, the first coordination sphere of sulfur in LZ40 (SCa_n) is isolated within the glass structure and yields only the first, singlet feature of the S *K*-edge XANES spectrum.

Glass LZ42 was synthesized from molar (6NAS + 1CaSO$_4$). The quenched product contained a minor amount of a sodalite-group phase (haüyne), present as inhomogeneously distributed <2 μm grains. This experiment may have simulated the not uncommon appearance of haüyne in alkali olivine basalt bombs, leucite trachytes and nephelinite lavas. The S *K*-edge XANES spectrum of LZ42 is dominated by a sharp edge-peak at about 2482 eV, corresponding to sulfate (S^{6+}); the extended XANES spectrum is similar to that of crystalline sulfate bonded to Ca^{2+} (*cf.* Figs. 1, 4; see also Fleet *et al.* 2005). However, the spectrum of LZ42 is considered to be fairly representative of the vitreous state, because the sodalite-group phase is present only in minor amount, and the geometry of the strongly bonded SO_4^{2-} tetrahedron will be essentially unchanged from gypsum, anhydrite and haüyne. This expectation is confirmed by the XANES spectrum of glass LZ50, which has a S^{6+} *K*-edge peak profile closely comparable to that of LZ42 (Fig. 4).

Experience shows that a sharp peak at about 2482 eV is a positive indication of the presence of sulfate species in complex S-bearing materials, and the size of the peak is proportional to the amount of sulfate present. Where two or more sulfur species are present in a glass, the S *K*-edge XANES spectrum will be composite of the separate absorption edges; *i.e.*, the XANES spectrum approximates to the weighted sum of the two or more absorption edges, because the absorption cross-section of the absorber atom is fairly independent of chemical state. Change in the appearance of S *K*-edge XANES spectra with variation in proportion of S^{2-} and S^{6+} is simulated by the summed spectra in Figure 5. Even where sulfate is only 10% of total sulfur species, it evidently results in a recognizable signature feature at 2482 eV.

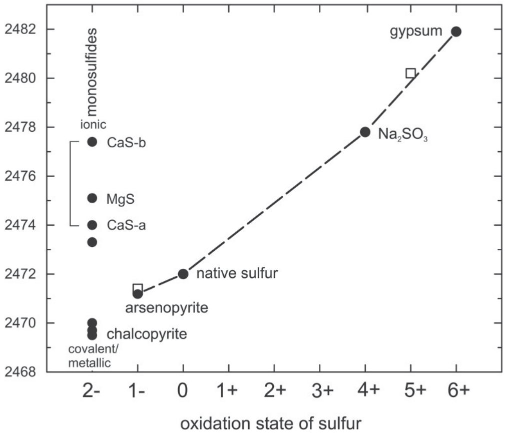

FIG. 2. Position of S *K* edge for some reference compounds and minerals showing a curvilinear correlation with oxidation state of sulfur for compositions ranging from covalent-metallic metal sulfides to gypsum, and the marked influence of bond character of the metal monosulfides: complex edge for CaS is indicated by peaks CaS–a and CaS–b (see Fig. 3); open squares locate the thio and "sulfate" edges of $Na_2S_2O_3$.

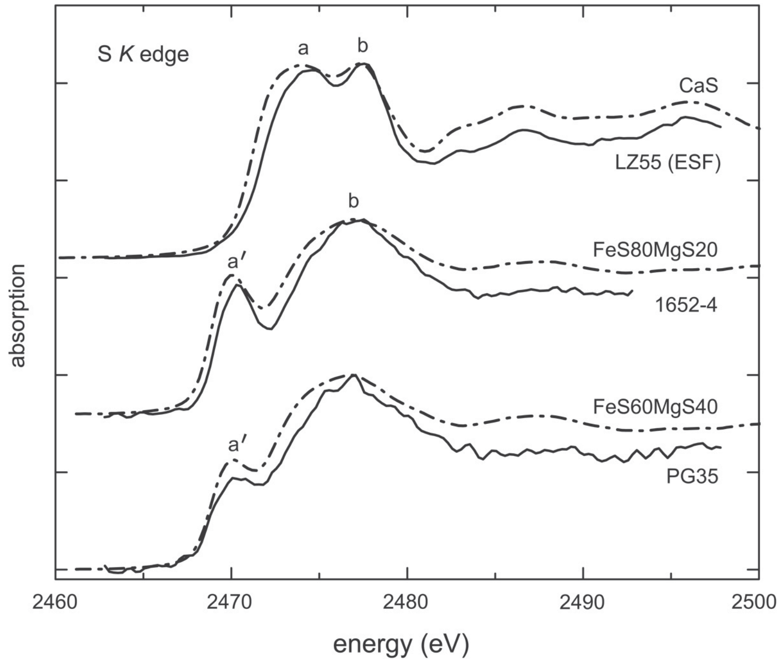

FIG. 3. Sulfur *K*-edge XANES spectra of CaS-bearing Na-aluminosilicate glass (LZ55; 0.75 wt% S), basaltic glass from the eastern Galapagos rift (1652–4; 0.11 wt% S), and synthetic basaltic glass (PG35; 0.08 wt% S), compared with spectra for synthetic oldhamite (cubic, halite-structured CaS), a mixture of 80 parts FeS and 20 parts MgS (synthetic niningerite), and a mixture of 60 parts FeS and 40 parts MgS, respectively. Glass spectra were recorded with the ESF detector, and the spectra of reference compounds were recorded with the conventional FY detector.

Starting compositions containing mixtures of CaS and $CaSO_4$ resulted in appreciable loss of sulfur, presumably from redox reactions of the type:

$$CaS + 3CaSO_4 \rightarrow 4CaO + 4SO_2 \quad (1)$$

The glass LZ50, which was synthesized from molar ($6NS + 0.1CaS + 0.9CaSO_4$), appears to have the requisite amount of sulfur by EPMA (Table 2), but this result was merely a reflection of the small content of CaS in the starting composition. The S *K*-edge XANES spectrum of LZ50 actually has only a very weak 2475 eV peak for reduced sulfur species (Fig. 4), compared with that expected for this bulk composition (Fig. 5).

Five glasses were synthesized with progressively decreasing amounts of CaS (LZ51 to LZ55; Table 2, Figs. 6, 7). As expected, the S *K*-edge XANES spectra recorded in FY mode are characterized by an edge peak near 2475 eV representing monosulfide bonded to Ca, although the spectra of LZ53 and LZ54 also indicate the presence of small amounts of sulfate, representing oxidation of the glass during sample preparation in air. This origin for the sulfate component is confirmed by the much greater prominence of the sulfate peak at 2482 eV in corresponding TEY XANES spectra; the TEY measurement probes only the subsurface of the glass powder, whereas FY is a bulk measurement. The variation of edge-peak area with sulfur content determined by EPMA is not linear, as expected; the areas for glasses of relatively low sulfur content (LZ55 and LZ54) plot below the calibration line in Figure 7. These discrepancies are attributed to crystallization or devitrification during quenching and probably also to incomplete melting of starting mixture(s) closest to the $NaAlSiO_4$ end-member composition, which has a melting point of 1526°C. The experimental temperature was restricted by the limited lifetime of the sealed silica-glass tubes above 1500°C. Glasses LZ51 and LZ52 are X-ray amorphous, but the other three experiments show evidence of crystallization, varying from a trace of powder-diffraction peaks due to carnegieite in LZ53 to minor carnegieite in LZ54 and extensive re-crystallization to carnegieite + minor oldhamite (CaS) in LZ55. Moreover, EPMA electron-back-scattering images of LZ55 revealed a texture of interlocking domains or grains of Na-aluminosilicate with domain or grain boundaries decorated by <1 μm grains of CaS. It appears that the synthetic oldhamite has quantitatively precipitated

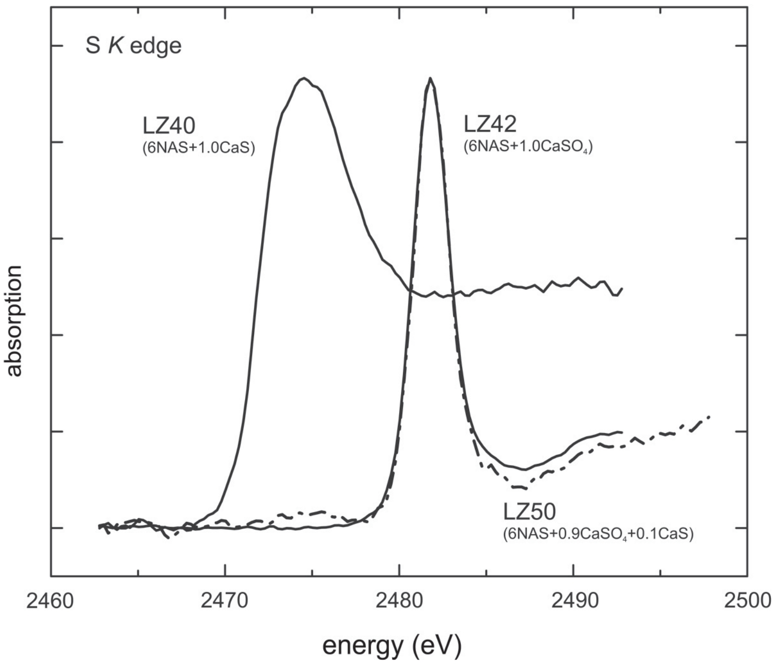

FIG. 4. Sulfur *K*-edge XANES spectra of quenched Na–Ca-aluminosilicate melts, showing pronounced shift in absorption edge from monosulfide (S^{2-}; LZ40) to sulfate (S^{6+}; LZ42) and loss of monosulfide in synthesis of LZ50 (dot-dashed spectrum): starting compositions were (6NAS + 1.0CaS) for LZ40, (6NAS + 1.0CaSO$_4$) for LZ42, and (6NAS + 0.9CaSO$_4$ + 0.1CaS) for LZ50; NAS is NaAlSiO$_4$. The spectra were recorded in FY mode.

from the melt during quenching. This conclusion is confirmed by the S *K*-edge XANES spectrum of LZ55 recorded in ESF mode, which is a very close match to the S XANES of crystalline halite-structured CaS (Fig. 3). It is now evident that the double-humped edge feature of the less well-resolved FY XANES of this glass (**a** and **b** in Fig. 6) also represents crystalline CaS, and contrasts markedly with the singlet edge feature of SCa$_n$ dissolved in Na-aluminosilicate glass (*e.g.*, LZ51 in Fig. 6). Assuming a linear correlation between XANES area and sulfur content, the XANES spectrum of LZ52 with 1.95 wt% S has been used to estimate major to minor amounts of sulfur in some silicate minerals, with reasonable success (Table 5). As described in Fleet *et al*. (2005), the S *K*-edge XANES spectra of the two natural samples of lazurite are a composite of dominantly sulfate with minor amounts of reduced sulfur species. Sulfate is the only species consistently present in S *K*-edge XANES spectra of the two samples of scapolite, but the TEY XANES spectra of scapolite 202 reveal minor reduced sulfur and sulfite in the sample subsurface.

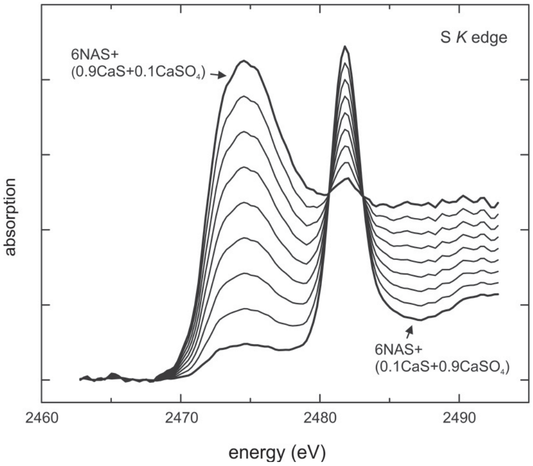

FIG. 5. Simulated S *K*-edge XANES spectra for Na–Ca-aluminosilicate glasses showing effect of change in proportion of CaS and CaSO$_4$ in the starting composition. Glass compositions range from 6NAS + (0.9CaS + 0.1CaSO$_4$) to 6NAS + (0.1CaS + 0.9CaSO$_4$), and are based on end-member spectra of LZ40 and LZ42 (*cf*. Fig. 4); NAS is NaAlSiO$_4$.

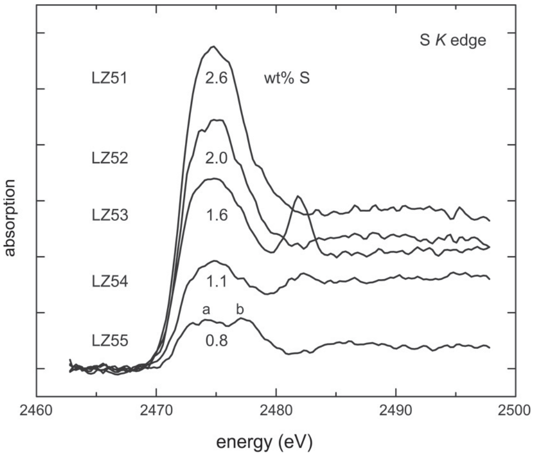

FIG. 6. Influence of progressive increase in sulfur content on S *K*-edge XANES spectra of CaS-bearing Na-aluminosilicate glasses: note that LZ51 replicates LZ40 (*cf.* Fig. 4, Table 1); **a** and **b** label the complex edge-feature of LZ55 (*cf.* XANES for crystalline CaS in Fig. 3). The spectra were recorded in FY mode.

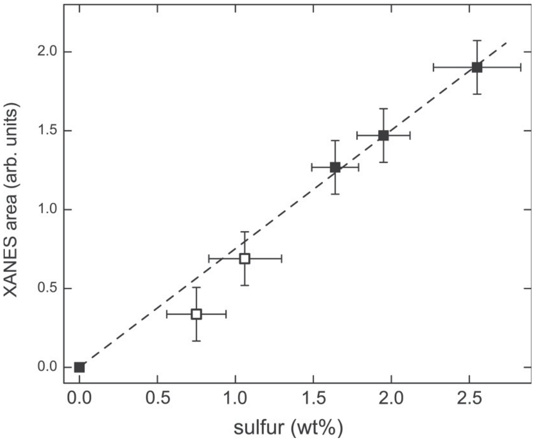

FIG. 7. Near-linear correlation of XANES peak area with content of sulfur in CaS-bearing Na-aluminosilicate glasses: S *K*-edge XANES spectra (recorded in FY mode) were sampled from 2466.3 to 2497.8 eV. The dashed line has been fitted visually; open squares flag glass products that were partially to extensively crystalline. Error bars represent ±1σ of EPMA data for sulfur content and estimates of reproducibility for XANES peak area.

Basaltic glasses

Selected S *K*-edge XANES spectra for the synthetic and Galapagos basaltic glasses are shown in Figures 3 and 8. These spectra were collected using the energy-selective fluorescence (ESF) detector and represent sulfur contents of 0.08 to 0.21 wt%. Compared with the micro-XANES spectra of basaltic glass fragments in Bonnin-Mosbah *et al.* (2002), the present ESF spectra have a similar resolution but a smoother overall profile in the 2470–2482 eV range, which results in superficial similarity to the S *K*-edge XANES spectra of the present CaS-bearing Na-aluminosilicate glasses (Figs. 4, 6). A ragged broad edge-feature similar in appearance to the micro-XANES spectra of Bonnin-Mosbah *et al.* (2002) is evident for sulfur contents of 0.05 wt% S and less. At any rate, conventional S *K*-edge XANES spectroscopy employing wide-beam synchrotron radiation is sufficiently sensitive to probe the 0.1 wt% levels of sulfur commonly encountered in mafic volcanic rocks and yields meaningful information on chemical state and content of sulfur. The minimum detection-limit for sulfur (*i.e.*, resolution of the S *K* edge above background) was not investigated systematically, but appears to be less than 0.01 wt%, although the information on chemical state at this low concentration would be very limited. The only sample measured using both ESF and FY methods of detection was LZ55 (0.75 wt% S; Table 2). The minimum detection-limits estimated from the signal noise of LZ55 spectra are ~0.01 wt% for ESF and ~0.07 wt% for FY. Also, the minimum detection-limit for S in the basalt glass PG34 (0.093 wt% S; Table 5) using the ESF mode was estimated similarly to be ~0.01 wt%.

The synthetic basaltic glasses were all quenched from melts having redox conditions close to the wüstite–magnetite (WM; PG34, PG35) and iron – quartz – fayalite (IQF; PG160R–PG176) solid oxygen buffers and stabilizing an immiscible liquid iron sulfide (Table 3). In addition to the broad edge-feature at 2470–2482 eV, their S *K*-edge XANES spectra have a weak peak or shoulder at 2470–2471 eV, which evidently corresponds to the S 1*s* → S 3*p* σ*/3*d*(e_g) transition (peak **a**) in NiAs-type (B8) FeS, and is presently labeled peak "**a'**". Peak **a'** does not appear to represent contamination by blebs of iron sulfide trapped in the glasses, because only traces of microblebs of sulfide were detected by optical microscopy and EPMA electron back-scattering, and this peak is clearly shifted to higher energy (2471 eV) in some of our glasses (Fig. 8). We conclude that these S *K*-edge XANES spectra represent monosulfide dissolved in the melts (glasses) and that peak **a'** is diminished and shifted in energy relative to the spectrum for $Fe_{0.923}S$ (Fig. 1) because the stereochemical environment of S^{2-} is different in the glass. Even if sulfur is bonded exclusively to iron atoms in the glass, the change in coordination, bonding character and electrical and magnetic properties would result in weaker hybridization of S 3*p* σ* antibonding and empty Fe 3*d* orbitals and diminution in size of peak **a'** and possibly displacement of **a'** as well. Moreover, the first coordination sphere of S in

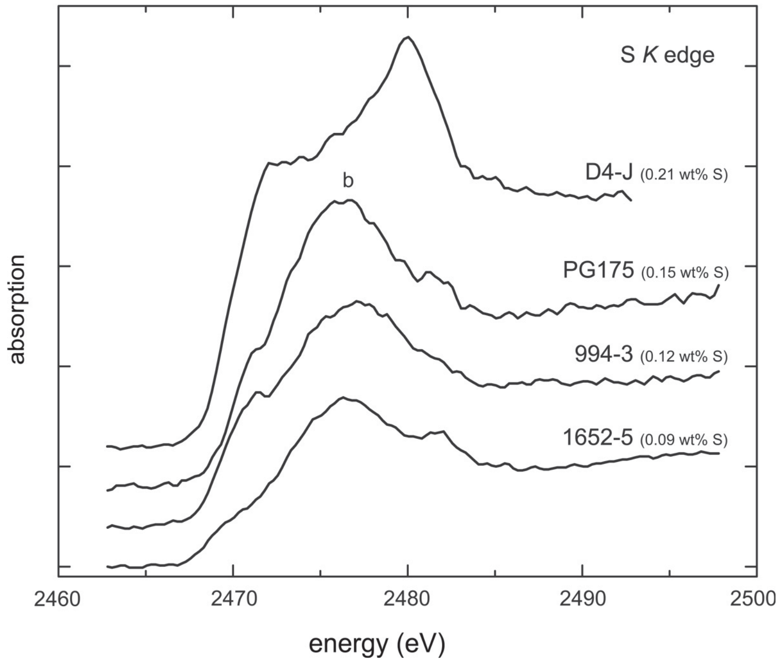

FIG. 8. Sulfur *K*-edge XANES spectra recorded in ESF mode for basaltic glasses from the eastern Galapagos rift (D4–J, 994–3, and 1652–5; Perfit *et al.* 1983, 1999) and a synthetic basaltic glass (PG175; Fleet *et al.* 1999). The spectra were recorded with the ESF detector.

basaltic glasses is likely to contain a small proportion of alkaline earth and alkali cations, particularly Ca^{2+}. For example, both Haughton *et al.* (1974) and O'Neill & Mavrogenes (2002) found that the molar content of CaO makes a significant contribution to the sulfur capacity of laboratory-equilibrated basaltic melts, CaO being, respectively, about 0.3 to 0.28 times as important as FeO in this respect. The contribution of CaO and other components to sulfur solubility is manifest in the plot of sulfur *versus* FeO in the melt in Haughton *et al.* (1974, Fig. 3), which extrapolates to about 0.04 wt% S in the melt at 0.0 wt% FeO. The potential for a mixed (Fe^{2+} + Ca^{2+}) nearest-neighbor shell for S in basaltic melts is supported by the simulated XANES spectra in Figure 3. The S *K*-edge XANES of PG35 (0.08 wt% S) is reproduced by mixing the spectra of NiAs-type FeS and cubic (B1) MgS in the ratio 3:2, and that of 1652–4 (0.11 wt% S), by mixing these sulfide spectra in the ratio 4:1. We have used the MgS XANES spectrum here as a proxy for CaS "dissolved in the glass", because the spectrum for the CaS reference compound (synthetic oldhamite) has a prominent second edge-feature (**b**) that is characteristic of the crystalline state (Fig. 3) but not present in spectra for CaS dissolved in silicate glasses (Fig. 4); the normalized XANES spectrum of either LZ40 (Fig. 4) or LZ51 (Fig. 6) yields a similar, albeit noisier, result. Clearly, even in the absence of change in the S–Fe bonding, as little as 20% Ca^{2+} in the nearest-neighbor shell of S reduces the size of the first edge-feature (peak **a'**) significantly, and 40% Ca^{2+} reduces it to a minor feature.

The S *K*-edge XANES spectra of the Galapagos glasses display a wider variation in features than the synthetic basaltic glasses (Figs. 3, 8), no doubt a reflection of more varied redox conditions, and quenching and cooling histories. Peak **a'** is fairly prominent for 1652–4 (0.11 wt% S; Fig. 3), but barely present for 1652–5 (0.09 wt% S; Fig. 8). Also, the spectrum of 1652–5 indicates a small amount of sulfate. The XANES spectrum of D4–J is distinctly different, having a prominent peak at 2480 eV and a prominent shoulder at about 2472 eV. We speculate that these two features represent thiosulfate from gases or hydrothermal fluids that overprinted D4–J during its cooling history. The thiosulfate complex has limited thermal stability ($Na_2S_2O_3$ disproportionates at 450°C), and is not expected to be present under magmatic conditions. Unfortunately, the micro-FTIR study of D4–J glass did not give results in support of this preliminary result, as measurable H_2O was detected but without detection of S–O species. This null result does not rule out the presence of thiosulfate because it is likely that ~0.1 wt% levels of S are below the minimum detection-limit for micro-FTIR and, in addition, there is spectral interference from strong Si–O vibrations.

The S *K*-edge XANES spectra for the present basaltic glasses equilibrated under reducing (WM and IQF oxygen buffer) conditions reveal only reduced sulfur species (presumably S^{2-}). In contrast, both sulfide and sulfate are present in *K*-edge XANES spectra for sulfur in some natural and synthetic glasses of basaltic to rhyolitic compositions representing more oxidizing redox conditions (Paris *et al.* 2001). The samples investigated have sulfur contents of 0.045 to 0.30 wt.%, and included a back-arc basalt, three samples of dacite from Mt. St. Helens equilibrated in the laboratory at 2–3 kbar and at the magnetite–hematite (MH) or Mn oxides (MNO) oxygen buffers, and an NBS standard Na–Ca silicate glass equilibrated in air. The sulfur speciation is dominantly sulfide with minor sulfate in the basalt, dominantly sulfate in the dacite samples, and exclusively sulfate in the NBS standard glass. Unlike the S *K*-edge XANES studies of Bonnin-Mosbah *et al.* (2002) and Métrich *et al.* (2002, 2003) on glass inclusions in olivine from oxidized and H_2O-rich basaltic arc magmas, the XANES spectra of the present reduced basaltic glasses reveal no evidence for a sulfite species, in the form of a sharp peak at about 2478 eV. The broad feature **b** (Figs. 3, 8) belongs to the monosulfide *K* edge and does not represent sulfur species of intermediate oxidation-state. Also, note that sulfur dissolved in silicate glasses is susceptible to oxidation during sample preparation and measurement, so that peaks for intermediate and oxidized sulfur species have to be checked for depth sensitivity by simultaneous TEY and FY measurements.

The low, minor contents of sulfur in the basaltic glasses have been estimated from the areas of their S *K*-edge XANES spectra, by assuming a linear correlation between XANES area and sulfur content, and normalizing against the XANES spectrum of PG175 with 0.15 wt% S (Table 5). The agreement with the EPMA results for these glasses is remarkably good, with the exception of anomalously high XANES values for PG160R and D4–J. Both of these glasses yielded atypical XANES spectra; contamination during sample preparation cannot be excluded. However, the content of sulfur in PG160R approaches the lower limit of detection by the XANES method, so that the anomaly here could represent experimental error. Sulfur appears to be distributed inhomogeneously in D4–J. As suggested above, this basaltic glass may have been locally contaminated in the abyssal ocean floor of the eastern Galapagos rift by gas or hydrothermal fluid that either was thiosulfate-bearing or reacted with the cooling rock to yield thiosulfate.

ACKNOWLEDGEMENTS

We thank Shannon Farrell and a second, anonymous reviewer for helpful comments, Michael Perfit for samples from the eastern Galapagos rift, Menghua Liu for assistance with EPMA, Astrid Jürgensen and Kim Tan, Canadian Synchrotron Radiation Facility, and staff of the Synchrotron Radiation Centre (SRC), University of Wisconsin at Madison, for their technical assistance, and the National Science Foundation (NSF) for support of the SRC under the grant #DMR–0084402. This work was supported by the Natural Sciences and Engineering Research Council of Canada, and the Canada Foundation for Innovation – Ontario Innovation Trust (PLK).

REFERENCES

BANCROFT, G.M. (1992): New developments in far UV, soft X-ray research at the Canadian Synchrotron Radiation Facility. *Can. Chem. News* **44**, 15-22.

BEAUCHEMIN, S., HESTERBERG, D. & BEAUCHEMIN, M. (2002): Principal component analysis approach for modeling sulfur K-XANES spectra of humic acids. *J. Soil Sci. Soc. Am.* **66**, 83-91.

BEERKENS, R.G.C. & KAHL, K. (2002): Chemistry of sulphur in soda–lime–silica glass melts. *Phys. Chem. Glasses* **43**, 189-198.

BONNIN-MOSBAH, M., MÉTRICH, N., SUSINI, J., SALOMÉ, M., MASSARE, D. & MENEZ, B. (2002): Micro X-ray absorption near edge structure at the sulfur and iron *K*-edges in natural silicate glasses. *Spectrochim. Acta B* **57**, 711-725.

CARROLL, M.R. & RUTHERFORD, M.J. (1988): Sulfur speciation in hydrous experimental glasses of varying oxidation state: results from measured wavelength shifts of sulfur X-rays. *Am. Mineral.* **73**, 845-849.

________ & WEBSTER, J.D. (1994): Solubilities of sulfur, noble gases, nitrogen, chlorine, and fluorine in magmas. *In* Volatiles in Magmas (M.R. Carroll & J.R. Holloway, eds.). *Rev. Mineral.* **30**, 231-279.

CLEMENTE, B., SCAILLET, B., PICHAVANT, M. & CARROLL, M.R. (1998): Solubility and speciation of sulphur as a function of fO_2 and fS_2 in silicic melts; toward a thermodynamic model. *Terra Abstr.* **10**, 8-9.

DUCEA, M.N., MCINNES, B.I.A. & WYLLIE, P.J. (1999): Experimental determination of compositional dependence of hydrous silicate melts on sulfate solubility. *Eur. J. Mineral.* **11**, 33-43.

FARRELL, S.P. & FLEET, M.E. (2000): Evolution of local electronic structure in cubic $Mg_{1-x}Fe_xS$ by S *K*-edge XANES spectroscopy. *Solid State Commun.* **113**, 69-72.

________ & ________ (2001): Sulfur K-edge XANES study of local electronic structure in ternary monosulfide solid solution [(Fe, Co, Ni)$_{0.923}$S]. *Phys. Chem. Minerals* **28**, 17-27.

________, ________, STEKHIN, I.E., KRAVTSOVA, A., SOLDATOV, A.V. & LIU, XIAOYANG (2002): Evolution of local electronic structure in alabandite and niningerite solid solutions [(Mn,Fe)S, (Mg,Mn)S, (Mg,Fe)S] using sulfur

K- and L-edge XANES spectroscopy. *Am. Mineral.* **87**, 1321-1332.

FINCHAM, C.J.B. & RICHARDSON, F.D. (1954): The behaviour of sulphur in silicate and aluminate melts. *Proc. R. Soc. London, Ser. A* **223**, 40-62.

FLEET, M.E., CROCKET, J.H, LIU, MENGHUA & STONE, W.E. (1999): Laboratory partitioning of platinum-group elements (PGE) and gold with application to magmatic sulfide – PGE deposits. *Lithos* **47**, 127-142.

________, LIU, XIAOYANG, HARMER, S.L. & NESBITT, H.W. (2005): Chemical state of sulfur in natural and synthetic lazurite by S *K*-edge XANES and X-ray photoelectron spectroscopy. *Can. Mineral.* **43**,

________ & MUTHUPARI, S. (2000): Coordination of boron in alkali borosilicate glasses using XANES. *J. Non-Cryst. Solids* **255**, 233-241.

________, ________, KASRAI, M. & PRABAKAR, S. (1997): Sixfold coordinated Si in alkali and alkali–CaO silicophosphate glasses by Si *K*-edge XANES spectroscopy. *J. Non-Cryst. Solids* **220**, 85-92.

FUGGLE, J.C. & INGLESFIELD, J.E., eds. (1992): *Unoccupied Electronic States: Fundamentals for XANES, EELS, IPS and BIS.* Springer-Verlag, New York, N.Y.

HAUGHTON, D.R., ROEDER, P.L. & SKINNER, B.J. (1974): Solubility of sulfur in mafic magmas. *Econ. Geol.* **69**, 451-467.

HITCHCOCK, A.P., BODEUR, S. & TRONC, M. (1987): Sulfur and chlorine K-shell X-ray absorption spectra of SCl_2, S_2Cl_2, $SOCl_2$ and SO_2Cl_2. *Chem. Phys.* **115**, 93-101.

HUFFMAN, G.P., MITRA, S., HUGGINS, F.E., SHAH, N., VAIDYA, S. & LU, F. (1991): Quantitative analysis of all major forms of sulfur in coal by X-ray absorption fine structure spectroscopy. *Energy Fuels* **5**, 574-581.

KASRAI, M., BROWN, J.R., BANCROFT, G.M., YIN, Z. & TAN, K.H. (1996a): Sulphur characterization in coal from X-ray absorption near edge spectroscopy. *Int. J. Coal Geol.* **32**, 107-135.

________, LENNARD, W.N., BRUNNER, R.W., BANCROFT, G.M., BARDWELL, J.A. & TAN, K.H. (1996b): Sampling depth of total electron and fluorescence measurements in Si L- and K-edge absorption spectroscopy. *Appl. Surf. Sci.* **99**, 303-312.

KATSURA, T. & NAGASHIMA, S. (1974): Solubility of sulfur in some magmas at 1 atmosphere. *Geochim. Cosmochim. Acta* **38**, 517-531.

KITAMURA, M., SUGIURA, C. & MURAMATSU, S. (1988): Multiple-scattering calculation of sulfur K X-ray absorption spectra for FeS, CoS and NiS. *Solid State Commun.* **67**, 313-316.

KRAVTSOVA, A.N., STEKHIN, I.E., SOLDATOV, A.V., LIU, X. & FLEET, M.E. (2004): Electronic structure of MS (M = Ca,Mg,Fe,Mn): X-ray absorption analysis. *Phys. Rev. B* **69**, 134109/1-134109/12.

LI, DIEN, BANCROFT, G.M., KASRAI, M., FLEET, M.E., FENG, XINGFONG & TAN, K. (1995): S K- and L-edge X-ray absorption spectroscopy of metal sulfides and sulfates: applications in mineralogy and geochemistry. *Can. Mineral.* **33**, 949-960.

LUHR, J.F. (1990): Experimental phase relations of water- and sulfur-saturated arc magmas and the 1982 eruptions of El Chichón Volcano. *J. Petrol.* **31**, 1071-1114.

MATHEZ, E.A. (1976): Sulfur solubility and magmatic sulfides in submarine basalt glass. *J. Geophys. Res.* **81**, 4269-4276.

MAVROGENES, J.A. & O'NEILL, H.S.C. (1999): The relative effects of pressure, temperature and oxygen fugacity on the solubility of sulfide in mafic magmas. *Geochim. Cosmochim. Acta* **63**, 1173-1180.

MÉTRICH, N., BONNIN-MOSBAH, M., SUSINI, J., MENEZ, B. & GALOISY, L. (2002): Presence of sulfite (S^{IV}) in arc magmas: implications for volcanic sulfur emissions. *Geophys. Res. Lett.* **29**, 33/1-33/4.

________, SUSINI, J., GALOISY, L., CALAS, G., BONNIN-MOSBAH, M. & MENEZ, B. (2003): X-ray microspectroscopy of sulfur in basaltic glass inclusions. Inference on the volcanic sulfur emissions. *J. Phys. IV: Proc.* **104**, 393-397.

MYSEN, B.O. & POPP, R.K. (1980): Solubility of sulfur in $CaMgSi_2O_6$ and $NaAlSi_3O_8$ melts at high pressure and temperature with controlled fO_2 and fS_2. *Am. J. Sci.* **280**, 78-92.

NALDRETT, A.J. (1989): *Magmatic Sulfide Deposits.* Clarendon Press, New York, N.Y.

O'NEILL, H.S.C. & MAVROGENES, J.A. (2002): The sulfide capacity and the sulfur content at sulfide saturation of silicate melts at 1400°C and 1 bar. *J. Petrol.* **43**, 1049-1087.

PARIS, E., GIULI, G., CARROLL, M.R. & DAVOLI, I. (2001): The valence and speciation of sulfur in glasses by X-ray absorption spectroscopy. *Can. Mineral.* **39**, 331-339.

PERFIT, M.R., FORNARI, D.J., MALAHOFF, A. & EMBLEY, R.W. (1983): Geochemical studies of abyssal lavas recovered by DSRV Alvin from eastern Galapagos rift, Inca transform, and Ecuador Rift. 3. Trace element abundances and petrogenesis. *J. Geophys. Res.* **88**, 10551-10572.

________, RIDLEY, W.I. & JONASSON, I.R. (1999): Geologic, petrologic, and geochemical relationships between magmatism and massive sulfide mineralization along the Eastern Galapagos Spreading Center. *In* Volcanic-Associated Massive Sulfide Deposits: Processes and Examples in Modern and Ancient Settings (C.T. Barrie & M.D. Hannington, eds.). *Rev. Econ. Geol.* **8**, 75-99.

SARRET, G., CONNAN, J., KASRAI, M., BANCROFT, G.M., CHARRIÉ-DUHAUT, A., LEMOINE, S., ADAM, P., ALBRECHT, P. & EYBERT-BÉRARD, L. (1999): Chemical forms of sulfur in geological and archeological asphaltanes from Middle East, France, and Spain determined by sulfur *K*- and *L*-edge X-ray absorption near-edge structure spectroscopy. *Geochim. Cosmochim. Acta* **63**, 3767-3779.

________, MONGENOT, T., CONNAN, J., DERENNE, S., KASRAI, M., BANCROFT, G.M. & LARGEAU, C. (2002): Sulfur speciation in kerogens of the Orbagnoux deposit (Upper Kimmeridgian, Jura) by XANES spectroscopy and pyrolysis. *Org. Geochem.* **33**, 877-895.

SOLDATOV, A.V., KRAVTSOVA, A.N., FLEET, M.E. & HARMER, S.L. (2004): Electronic structure of MeS (Me=Ni, Co, Fe): x-ray absorption analysis. *J. Phys.: Condensed Matter* **16**, 7545-7556.

SUGIURA, C. & MURAMATSU, S. (1985): Sulfur K X-ray absorption-edge structures and electronic states of transition-metal sulfides MS and MS_2 (M = Fe, Co, Ni). *Phys. Stat. Solidi B* **129**, K157-K161.

TOSSELL, J.A. (1977): SCF-X_α scattered wave MO studies of the electronic structure of ferrous iron in octahedral coordination with sulfur. *J. Chem. Phys.* **66**, 5712-5719.

TYLISZCAK, T. (1992): *BAN Data Analysis Program.* McMaster University, Hamilton Ontario.

VAIRAVAMURTHY, A. (1998): Using X-ray absorption to probe sulfur oxidation states in complex molecules. *Spectrochim. Acta A* **54**, 2009-2017.

________, MANOWITZ, B., LUTHER, G.W., III & JEON, Y. (1993a): Oxidation states of sulfur in thiosulfate and implications for anaerobic energy metabolism. *Geochim. Cosmochim. Acta* **57**, 1619-1623.

________, ________, ZHOU, W. & JEON, Y. (1993b): Determination of hydrogen sulfide oxidation products by sulfur K-edge X-ray absorption near-edge structure spectroscopy. *In* Environmental Geochemistry of Sulfide Oxidation (C.N. Alpers & D.W. Blowes, eds.). *Am. Chem. Soc., Symp. Ser.* **550**, 412-430.

WALDO, G.S., CARLSON, R.M.K., MOLDOWAN, J.M., PETERS, K.E. & PENNER-HAHN, J.E. (1991): Sulfur speciation in heavy petroleums: information from X-ray absorption near-edge structure. *Geochim. Cosmochim. Acta* **55**, 801-814.

WALLACE, P. & CARMICHAEL, I.S.E. (1992): Sulfur in basaltic magmas. *Geochim. Cosmochim. Acta* **56**, 1863-1874.

WOMES, M., KARNATAK, R.C., ESTEVA, J.M., LEFEBVRE, I., ALLAN, G., OLIVIER-FOURCADE, J. & JUMAS, J.C. (1997): Electronic structures of FeS and FeS_2: X-ray absorption spectroscopy and band structure calculations. *J. Phys. Chem. Solids* **58**, 345-352.

YANG, B.X., MIDDLETON, F.H., OLSSON, B.G., BANCROFT, G.M., CHEN, J.M., SHAM, T.K.,TAN, K. & WALLACE, D.J. (1992): The design and performance of a soft X-ray double crystal monochromator beamline at Aladdin. *Nucl. Instrum. Methods Phys. Res. A* **316**, 422-436.

Received August 31, 2004, revised manuscript accepted April 1, 2005.